

Results and achievements at CLAS

Silvia Pisano¹
(for the CLAS collaboration)

Laboratori Nazionali di Frascati - Via E. Fermi,40 – I-00044 Frascati (Rome) Italy

Abstract. This proceeding presents an overview of the main measurements of Generalized Parton Distributions (GPD) performed by the CLAS Collaboration. GPDs are experimentally accessed through exclusive processes like Deeply-Virtual Compton Scattering (DVCS) and Deeply-Virtual Meson Production (DVMP). The *CEBAF Large Acceptance Spectrometer* (CLAS) installed in the Hall-B of Jefferson Lab, with its large acceptance, is particularly suitable for the reconstruction of exclusive final states, allowing the investigation of these processes in a wide range of kinematics. In the following, an overview of the main results is given.

Keywords: Hadronic Physics; Generalized Parton Distributions; Nucleon Structure.

PACS: 25.20.Lj, 13.30.-a, 13.60.Le, 14.20.Gk, 14.40.Aq

INTRODUCTION

A complete description of hadrons in terms of their elementary constituents, quarks and gluons, is one of the main challenges of the present hadronic physics. In order to gain a better understanding of the hadron properties a new tool has been introduced some decades ago, the so-called *Generalized Parton Distributions* (**GPDs**) [1, 2], that, by combining the information coming from the electromagnetic form factors and from the standard parton distributions, allow a full, 3-dimensional description of the hadrons in terms of their partonic degrees of freedom. The best way to experimentally access these quantities is based on the so-called “*handbag*” mechanism and is expected to dominate processes as *Deeply Virtual Compton Scattering* (**DVCS**) and *Deeply Virtual Meson Production* (**DVMP**). For DVCS with transverse photons and DVMP with longitudinal photons, indeed, this picture has been proven through the use of factorization theorems [1, 2, 3]: the underlying mechanism can be separated in a hard scattering part, well described through the tools of *Quantum Electrodynamics* and/or *Quantum Chromodynamics*, and a non-perturbative part, that encodes the complex strong dynamics governing the existence of the hadron bound states and that is described with GPDs.

The actual extraction of GPDs goes through the introduction of asymmetries as

$$A = \frac{d^4\vec{\sigma} - d^4\overleftarrow{\sigma}}{d^4\vec{\sigma} + d^4\overleftarrow{\sigma}} \quad (1)$$

(the arrows corresponding to beam helicity +1 and -1), that is related to the GPDs H , \tilde{H} and E through $d^4\vec{\sigma} - d^4\overleftarrow{\sigma} \sim \sin\phi [F_1 H(\xi, \xi, t) + k_1(F_1 + F_2)\tilde{H}(\xi, \xi, t) + k_2 F_2 E(\xi, \xi, t)]$.

¹ silvia.pisano@lnf.infn.it

F_1 , F_2 are the Dirac and Pauli form factors of the nucleon, k_1 , k_2 are kinematical quantities, and ϕ is the angle between the $\gamma^* \gamma$ plane and the electron scattering plane.

Another process adopted in the GDP extraction is the Deeply Virtual Meson Production: by measuring different channels, indeed, a flavor-decomposition can be operated, allowing the access to the GPDs of every single quark flavour.

The results reported in this proceeding come mainly from two experiments: e1-6 and e1-dvcs. For the former, data were collected in 2001 and 2002 by using a 5.754 GeV electron beam impinging on an unpolarized 5-cm-long liquid-hydrogen target, for a total integrated luminosity of 28.5 fb^{-1} . The latter, e1-dvcs, was the first Hall-B experiment completely devoted to the DVCS analysis. It made use of a 5.77 GeV electron beam, a 2.5 cm-long liquid-hydrogen target and the CEBAF Large Acceptance Spectrometer (CLAS) [15], operating at a luminosity of $2 \times 10^{34} \text{ cm}^{-2}\text{s}^{-1}$. A new inner calorimeter was added to the standard CLAS configuration to detect high energy DVCS photons. Recently, another experiment dedicated to DVCS has been performed with a 6 GeV polarized electron beam and a polarized $^{14}\text{NH}_3$ target (eg1-dvcs), to study single and double spin asymmetries in the DVCS process, and analyses of these new data are ongoing.

CLAS RESULTS

The main results from the CLAS experiments has been the extraction of the Beam-Spin Asymmetry (BSA) for DVCS, reported in Fig. 1. All the three particles composing the $ep \rightarrow e'p'\gamma$ final state were detected, and the background was reduced through the application of exclusivity cuts. The data were divided into thirteen bins in the (x_B, Q^2) space, five bins in $-t$ (defined by the bin limits 0.09, 0.2, 0.4, 0.6, 1 and 1.8 GeV^2) and twelve 30° bins in ϕ . A couple of examples of the measured asymmetry are shown in Fig. 1, together with $a = A(90^\circ)$ as a function of $-t$. Two fits are superimposed to the experimental data, one corresponding to the hadronic model proposed in Ref. [16], and the other corresponding to the GPD calculation of Ref. [11].

As to the DVMP, one of the main CLAS results is represented by the measurements of the longitudinal cross-section for the process $ep \rightarrow e'p'\rho^0$ (Ref. [20]), whose results are reported in Fig. 2. They show $\gamma_L^* p \rightarrow p\rho_L^0$ as a function of W for constant Q^2 bins, together with the world data. The dot-dashed curve superimposed to the data represents a fit obtained with the Regge JML calculation [4, 5, 6, 7], while the dashed and the thin/thick solid curves represent fits obtained within GPD inspired models, in particular the VGG [8, 9, 10, 11] and the GK [13] ones. In these last two models the (x, ξ) dependence of the H and E GPDs is described through a double distribution (cfr. Ref. [21]), but they differ in the t -dependence and in the way they sum up the quark and gluon contribution to the handbag diagram. In the GK case, indeed, the two diagrams are combined at the *amplitude* level, while in the VGG model the sum occurs at the *cross section* level (neglecting, in this way, the interference between the terms). By looking at the data in Fig. 2, two different behaviours can be appreciated for the cross-section: at low W σ_L decreases with W , while it starts to rise again at $W \approx 10 \text{ GeV}$. The JML model reproduces fairly well these two general behaviours, but it drops as a function of Q^2 faster than the data and agrees only up to $Q^2 \approx 4.10 \text{ GeV}^2$. The GPD-based models,

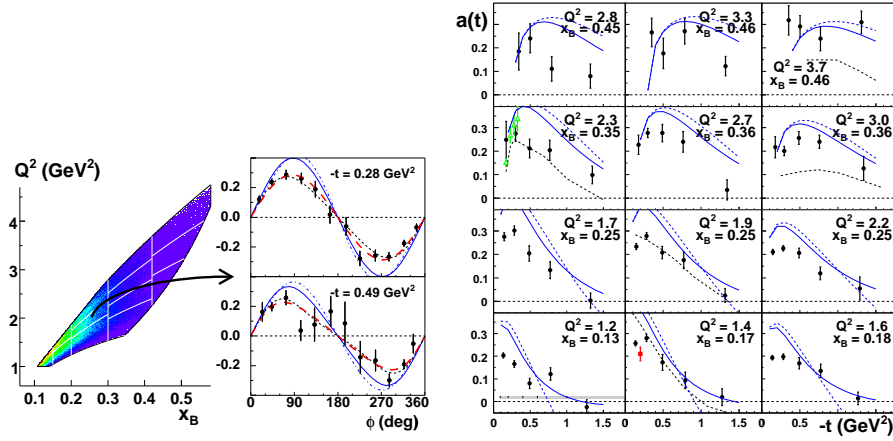


FIGURE 1. Left: kinematic coverage and binning in the (x_B, Q^2) space, together with $A(\phi)$ for 2 of the 62 (x_B, Q^2, t) bins, corresponding to $\langle x_B \rangle = 0.249$, $\langle Q^2 \rangle = 1.95 \text{ GeV}^2$, and two values of $\langle t \rangle$ ([17]). The black dashed curves correspond to a Regge calculation [16], while blue curves correspond to GPD calculation at twist-2 (solid) and twist-3 (dot-dashed) levels, with H contribution only. The red long-dashed curves correspond to fits with $A = \frac{a \sin \phi}{1 + c \cos \phi}$. Right: $a = A(90^\circ)$ as a function of $-t$. Each individual plot corresponds to a bin in (x_B, Q^2) . Systematic uncertainties and bin limits are illustrated by the grey band in the lower left plot. Black circles are from Ref. [17]. Previous CLAS results are from Ref. [18] (red square) or extracted from cross section measurements [19] (green triangles), at similar - but not equal - values of $\langle x_B \rangle$ and $\langle Q^2 \rangle$. Curve legend is the same as above.

on the other hand, give a good description of the high and intermediate W region, down to $W \approx 5 \text{ GeV}$.

As to the other mesons, CLAS measured exclusive electroproduction of ω [26] and ϕ [27]. Preliminary results for the ρ^+ are also available [28]. In Fig. 2 (right), the slopes of the differential cross section $d\sigma/dt$ for the ρ^0 , ω , ϕ and ρ^+ channels are shown as a function of W (top) and Q^2 (bottom). The same behaviour can be appreciated for all the channels: the increase of b with W can be addressed to the fact that the size of the nucleon increases as one probes the high W values (i.e. sea quarks tend to extend to the periphery of the nucleon), while its decrease with Q^2 can be explained by the fact that, going to large Q^2 , the probe resolution increases and smaller objects can be resolved.

CONCLUSION

GPDs are an essential tool for the comprehension of the nucleon structure. CLAS, the detector installed in the Hall-B at JLab, thanks to its large acceptance and the capability of a full, exclusive reconstruction of final states, is one of the most natural environment to measure processes as DVCS and DVMP, fundamental to access experimentally to GPDs. Results from the e1-dvcs experiment, based on the largest set of DVCS data currently available, show the expected sinusoidal dependence on ϕ for the beam-spin asymmetry, while the measure of the cross-section for ρ^0 , ω , ϕ and ρ^+ electroproduction allows to test the phenomenological power of the present existing GPD models and to constrain them.

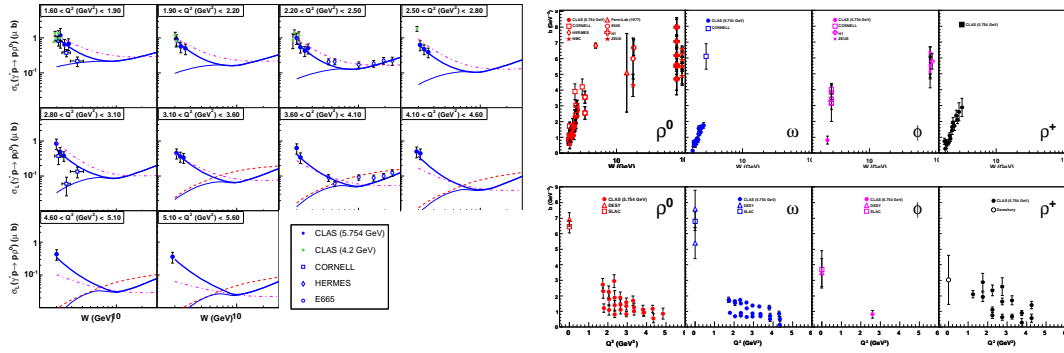


FIGURE 2. Left: World data for the reduced cross sections of the reaction $\gamma_L^* p \rightarrow p\rho_L^0$ as a function of W for constant Q^2 bins, in units of μbarn . The dashed curve shows the result of the GK calculation and the thin solid curve shows the result of the VGG calculation. Both calculations are based on Double Distributions as proposed in Ref. [21] for the GPD parametrizations and incorporate higher twist effects through k_\perp dependence. The thick solid curve is the VGG calculation with the addition of the D-term inspired contribution. The dot-dashed curve shows the results of the Regge JML calculation. The 4.2 GeV CLAS, CORNELL, HERMES and E665 data are respectively from refs. [22], [23], [24] and [25]. Right: b as a function of W (on the top) and as a function of Q^2 (on the bottom) for the ρ^0 , ω , ϕ and ρ^+ channels (the last one is a preliminary result).

REFERENCES

1. X. Ji, Phys. Rev. Lett. **78** (1997) 610; Phys. Rev. D **55** (1997) 7114.
2. J.C. Collins, L. Frankfurt and M. Strikman, Phys. Rev. D **56** (1997) 2982.
3. D. Müller, D. Robaschik, B. Geyer, F.-M. Dittes, and J. Horejsi, Fortschr. Phys. **42** (1994) 101.
4. J. M. Laget, Phys. Rev. D **70** (2004) 054023.
5. J.-M. Laget, Phys. Lett. B **489** (2000) 313.
6. F. Cano and J.-M. Laget, Phys. Rev. D **65** (2002) 074022.
7. F. Cano and J. M. Laget, Phys. Lett. B **551** (2003) 317.
8. M. Vanderhaeghen, P.A.M. Guichon, and M. Guidal, Phys. Rev. Lett. **80** (1998) 5064.
9. M. Vanderhaeghen, P.A.M. Guichon, and M. Guidal, Phys. Rev. D **60** (1999) 094017.
10. K. Goeke, M.V. Polyakov and M. Vanderhaeghen, Prog. Part. Nucl. Phys. **47** (2001) 401.
11. M. Guidal, M.V. Polyakov, A.V. Radyushkin and M. Vanderhaeghen, Phys. Rev. **D72** (2005) 054013.
12. A.V. Radyushkin, Phys. Lett. B **380** (1996) 417; Phys. Rev. D **56** (1997) 5524.
13. K. Goeke, M. V. Polyakov and M. Vanderhaeghen, Prog. Part. Nucl. Phys. **47** (2001) 401.
14. A.V. Belitsky and A.V. Radyushkin, Phys. Rept. **418** (2005) 1.
15. B. A. Mecking et al. Nucl. Instr. Meth. **A503** (2003) 513.
16. J. M. Laget, Phys. Rev. C **76** (2007) 052201.
17. F.X. Girod, Phys.Rev.Lett. **100** (2008) 162002.
18. S. Stepanyan et al. Phys. Rev. Lett. **87** (2001) 182002.
19. C. Muñoz Camacho et al., Phys. Rev. Lett. **97** (2006) 262002.
20. S. Morrow et al., Eur. Phys. J. A **39** (2009) 5.
21. A.V. Radyushkin, Phys. Rev. D **59** (1999) 014030; Phys. Lett. B **449** (1999) 81.
22. C. Hadjidakis *et al.*, Phys. Lett. B **605** (2005) 256.
23. D.G. Cassel *et al.*, Phys. Rev. D **24** (1981) 2787.
24. A. Airapetian *et al.*, Eur. Phys. J. C **17** (2000) 389.
25. M. R. Adams *et al.*, Z. Phys. C **74** (1997) 237.
26. L. Morand et al., Eur. Phys. J. A **24** (2005) 445.
27. J. P. Santoro et al., Phys. Rev. C **78** (2008) 025210.
28. A. Fradi, thesis Univ. Paris-Sud at Orsay, 2009.